Acta Cryst. (1976). A32, 558

Superstructures in an Imperfectly Quenched Vanadium Monosulphide, $VS_{1.155}$, as Observed by High-Resolution Electron Microscopy

BY SHIGEO HORIUCHI, ISAO KAWADA, MITSUKO NAKANO-ONODA, KATSUO KATO AND YOSHIO MATSUI
National Institute for Researches in Inorganic Materials, Sakura-mura, Niihari-gun, Ibaraki, Japan 300-31

AND FUMIO NAGATA
Hitachi Central Research Laboratory, Kokubunji, Tokyo, Japan 185

AND MITSUOKI NAKAHIRA
Okayama College of Science, Laboratory for Solid State Chemistry, Ridai-cho, Okayama, Japan 700

(*Received* 9 *May* 1975; *accepted* 12 *January* 1976)

The contrast of electron microscope lattice images of a vanadium monosulphide with superstructures was dynamically calculated on the basis of the multislice method. Interactions of 80 waves were analysed. It was shown that the vacancy-rich vanadium sites were imaged as white spots not only at the very thin part but also at the thicker part inside the first equal-thickness contour, which appeared at the thickness of 60 Å. A non-stoichiometric vanadium monosulphide, $VS_{1.155}$, quenched imperfectly from the preparation temperature at 1217 °C, was examined on the basis of the lattice image observation by a 100 kV high-resolution electron microscope. Orderings in the inter- as well as intralayers could be recognized directly from the arrangement of the white spots. Interpretable lattice images appeared exclusively inside the first equal-thickness contour. A mixture of some different types of images was observed in a crystal fragment; in some band-like regions the 4*C*-type superstructure was found with almost the same structure as Fe_7S_8. Each band extended parallel to the (001) plane with thickness of at most 50 Å and the orientation was in a twin relation to that of the adjoining one. The other regions showed less well-defined lattice images, although they gave the broad diffraction peaks ranging from the 4*C*- to 3*C*-type reflexions. In order to determine the phase relations at high temperatures the specimen was heated by focusing an electron beam on the portion slightly apart from the area under examination. The technique enabled us to observe only the heating effect. Upon heating, the 4*C* type first increased in volume, seen by the thickening of some bands. On further heating the 3*C* type increased in intensity on the diffraction pattern. The structure of the 3*C* type was estimated to be almost the same as Fe_7Se_8 except that the vacancy concentration fluctuated among the partially occupied vanadium layers.

Introduction

The lattice-image technique for studying crystal defects by high-resolution electron microscopy has recently been developed (Allpress, Sanders & Wadsley, 1969; Iijima, 1971, 1973; Uyeda, Kobayashi, Suito, Harada & Watanabe, 1972; Horiuchi & Matsui, 1974). The technique was successfully applied for characterizing crystal imperfections such as crystallographic shear planes, intergrowth defects, microtwins and point defects (Allpress & Sanders, 1973; Iijima, Kimura & Goto, 1973). It has been of great use especially in detecting the lattice defects, existing non-periodically in real crystals, which are difficult to resolve by other means (Buseck & Iijima, 1974; Horiuchi, Matsui, Kato & Nagata, 1975).

Many studies have been performed on the phase relations and crystal structures of vanadium sulphides (Grønvold, Haraldsen, Pedersen & Tufte, 1969; DeVries, 1972; Kawada, Nakano-Onoda, Ishii, Saeki & Nakahira, 1975). Vanadium monosulphides, VS_x, with a NiAs-type structure are stable in a wide composition range and often form superstructures of various types depending on temperature and composition. When specimens were prepared at temperatures higher than about 1000 °C and then cooled rapidly (Nakano-Onoda & Nakahira, 1976), they gave some diffuse peaks on the X-ray powder diffractometer charts for a composition range of $x=1{\cdot}07$ to $1{\cdot}18$ as well as fundamental reflexions of NiAs-type. It was considered that high-temperature phases could not be quenched perfectly and a mixture of some superstructures belonging to the lower temperature ranges at the same composition were formed during cooling.

The present study is concerned with a vanadium monosulphide of composition $x=1{\cdot}155$, prepared at 1217 °C and cooled rapidly. The lattice images formed by a high-resolution electron microscope were utilized to reveal the degree of mixing of superstructures and the distribution of lattice defects in the imperfectly quenched sulphide. Phase transitions were then deliberately introduced under observation, through raising the temperature of the specimen by increasing the electron beam intensity. The structural changes in the images as well as in the diffraction patterns throughout the above process were examined.

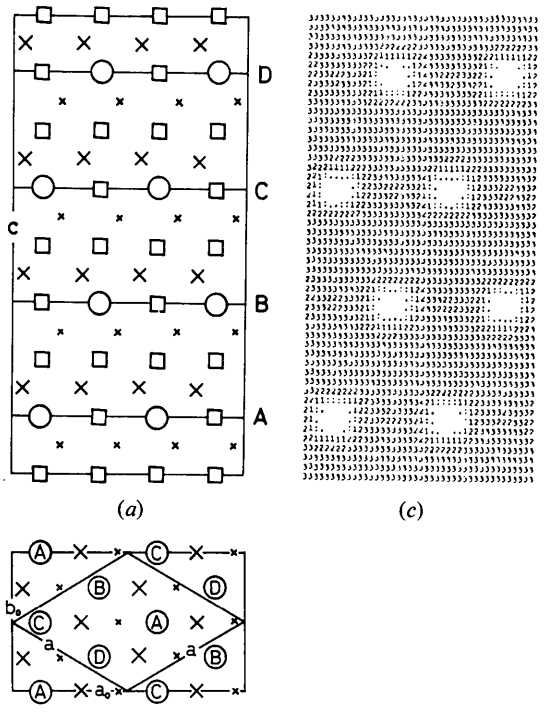

Fig. 1. Unit-cell of V_7S_8 with 4*C*-type superstructure. (*a*) Its projection in the $\mathbf{b}_o$ axis direction and (*b*) in the **c** axis direction. *A*, *B*, *C* and *D* show the positions of the partially occupied vanadium layers with ordered vacancies. $a=6{\cdot}7$ and $c=23{\cdot}2$ Å. (*c*) Computer simulation image, calculated for crystal thickness of 120 Å at an underfocus of 900 Å with spherical aberration coefficient of 2·0 mm. The objective aperture is assumed to be the medium one in Fig. 2.

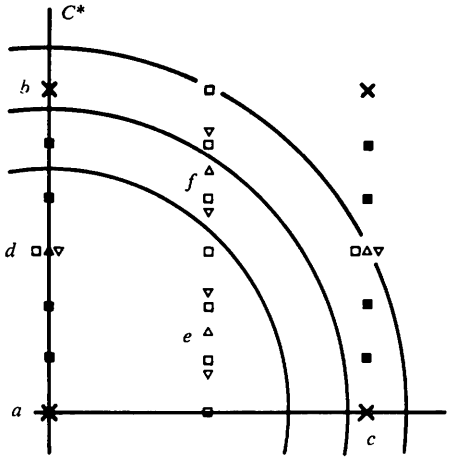

Fig. 2. Schematic representation of diffraction spots. Crosses show the fundamental reflexions from the NiAs subcell. The reflexions *b* and *c* are indexed as 002 and 100 based on the subcell, respectively. Other reflexions are excited by the superstructure; those indicated by up- and downward triangles are obtained from the 4*C* type with matrix and twin orientations respectively. Squares are from the 3*C*-type superstructure. Large circles indicate the objective aperture assumed in the computer simulation.

According to the kinematical theory of scattering the lattice images with a phase contrast taken at the so-called optimum defocus (Scherzer, 1949; Eisenhandler & Siegel, 1966), approximately reflect the projected potential of the crystal (Cowley & Iijima, 1972). The image contrast can sometimes be interpreted intuitively on the basis of the crystal structure. However, this holds only for very thin specimens. For crystals composed of medium-weight atoms, of more than about 10 Å thick, a dynamical scattering must be taken into account (Lynch, Moodie & O'Keefe, 1975). For sulphide crystals, as in the present case, interpretable lattice images usually appear inside the first equal-thickness contour at the edge of the crystal fragment, as will be shown. It is necessary to calculate the scattering amplitude taking account of crystal thickness in order to interpret the image contrast correctly.

Calculation of lattice image contrast of a vanadium monosulphide with a 4*C*-type superstructure

The superstructure model of vanadium monosulphides has so far been proposed only for V_7S_8 ($x=1{\cdot}143$), which has hexagonal symmetry with unit cell $a=2A$ and $c=4C$, where A and C are the lattice parameters of the NiAs subcell. Fig. 1(*a*) and (*b*) shows the projections of the unit cell in the [110] and [001] directions, respectively (DeVries, 1972). Squares and crosses represent the positions of vanadiums and sulphurs respectively. Circles represent the positions where every second vanadium atom is removed in the [110] direction. This is substantially the same superstructure as proposed originally for Fe_7S_8 by Bertaut (1953). Vacancies are confined only to every second vanadium layer to form so-called interlayer ordering. Moreover, they array regularly in the partially occupied vanadium layers, which are denoted by V_A, V_B, V_C and V_D. The stacking sequence of layers along the **c** axis is then represented as $\ldots V_AS_1VS_2V_BS_1VS_2V_CS_1VS_2V_DS_1VS_2V_A\ldots$, where V represents the fully occupied vanadium layer, and S_1 and S_2 the sulphur layers indicated by large and small crosses. It is hereafter referred to as $\ldots V_AV_BV_CV_DV_A\ldots$ for simplicity.

On computing the contrast of the lattice image it is convenient to take the orthogonal axes as drawn in Fig. 1(*b*). The lattice parameters are: $a_o=2\sqrt{3}A$ and $b_o=2A$ and $c_o=4C$. These orthogonal axes are considered only in this section. The original hexagonal axes are used again from the next section onwards. In order to detect lattice defects such as stacking faults in the crystal, it is considered most efficient to observe the lattice image with the incident beam parallel to the $\mathbf{b}_o$ axis. In this case the reflexions indicated by upward triangles in Fig. 2 will be excited.

The scattering amplitude of each reflexion was calculated dynamically based on the multislice method (Allpress & Sanders, 1973; O'Keefe, 1973), derived

originally by Cowley & Moodie (1957); the Fourier transform of the wave function for the $(n+1)$th slice, $u_{n+1}(h,l)$, is

$$u_{n+1}(h,l)=p_n(h,l)u_n(h,l)*q_{n+1}(h,l),$$

where $p(h,l)$ is the Fourier transform of the propagation function and $*$ is the convolution symbol. $p(h,l)$ is given by

$$p(h,l)=\exp[i2\pi\Delta y\xi(h,l)],$$

where Δy is the thickness of a slice and $\xi(h,l)$ the excitation error of the h,l beam. $q(h,l)$ is the Fourier transform of the transmission function of a slice, $\exp[i\sigma\varphi(x,z)]$, in which $\varphi(x,z)$ is the projected potential. $\sigma=\pi/\lambda E$, where λ and E are the wavelength and the accelerating voltage corrected for the relativistic effect, respectively. $q(h,l)$ was evaluated from the M times repeated convolution of A, *i.e.* $\ldots*A*A*A*\ldots$, where A is given by (Goodman & Moodie, 1974)

$$A=\delta(h,l)+i\sigma\mathscr{F}[\varphi(x,z)]/M.$$

$\mathscr{F}$ denotes a Fourier transformation. $M=1024$ and $\Delta y=|\mathbf{b}_o|=6{\cdot}7$ Å in the present calculation.

The amplitude at the bottom surface of crystal, $Q(h,l)$, was obtained from the repeated convolution and multiplications based on the equation

$$\ldots p_4\{p_3[p_2(p_1q_1*q_2)*q_3]*q_4\}*\ldots.$$

The interaction of 80 waves was taken into account. The intensity and phase obtained for some of reflexions are represented for thickness up to 500 Å in Fig. 3(*a*) and (*b*).

The intensity of the 000 spot [curve *a* in Fig. 3(*a*)] first decreases with the increase of thickness and reaches the first minimum point at the thickness of about 60 Å, where the first equal-thickness contour will appear in the image. It is interesting to note that the reflexions *d*, *e* and *f* change in a similar way in intensity as well as in phase up to a considerable thickness (~250 Å).

The complex amplitude of the scattered waves at the back focal plane is that above multiplied by $\exp(i\chi)$. χ is the phase factor given by

$$\chi=(2\pi/\lambda)[(\Delta f\alpha^2/2)-(C_s\alpha^4/4)]$$

where Δf represents the amount of defocus, α the scattering angle and C_s the spherical aberration coefficient.

The amplitude of electron waves in the image plane is attained by the inverse Fourier transformation of $R(h,l)Q(h,l)\exp(i\chi)$. $R(h,l)$ is the aperture function, *i.e.* 1 if the wave passes through the objective aperture and 0 otherwise. The intensity, I, is obtained by multiplying by the complex conjugate. The simulation image was drawn by plotting the values of $(I-I_{min})/(I_{max}-I_{min})$ on a scale of six steps at positions on the image plane.

Simulation images were computed for a series of crystal thicknesses taking into consideration defocus

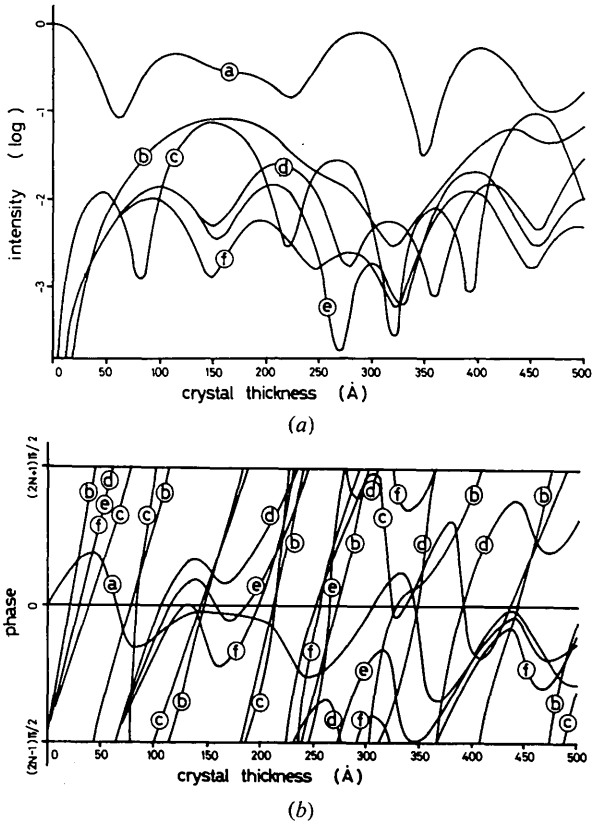

Fig. 3. (*a*) Intensity and (*b*) phase *versus* crystal thickness, calculated for the 4*C*-type superstructure of V_7S_8 in Fig. 1. The electrons are incident parallel to the $\mathbf{b}_o$ direction. The letters *a* to *f* mean the reflexions marked *a* to *f* in Fig. 2. The intensity of the incident electron beam is taken as unity. The phases are shown on a reduced scale. *N* is an integer.

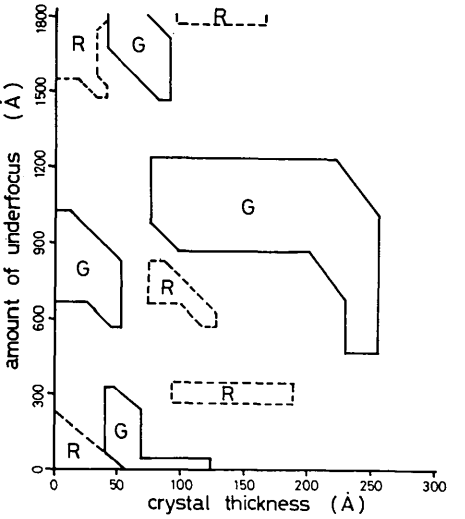

Fig. 4. The areas *G* show the extent of thickness and defocus in which the rows of vacancies are imaged as white spots. The areas *R* show the extent to which the image contrast is reversed. The objective aperture is assumed to be the medium one in Fig. 2.

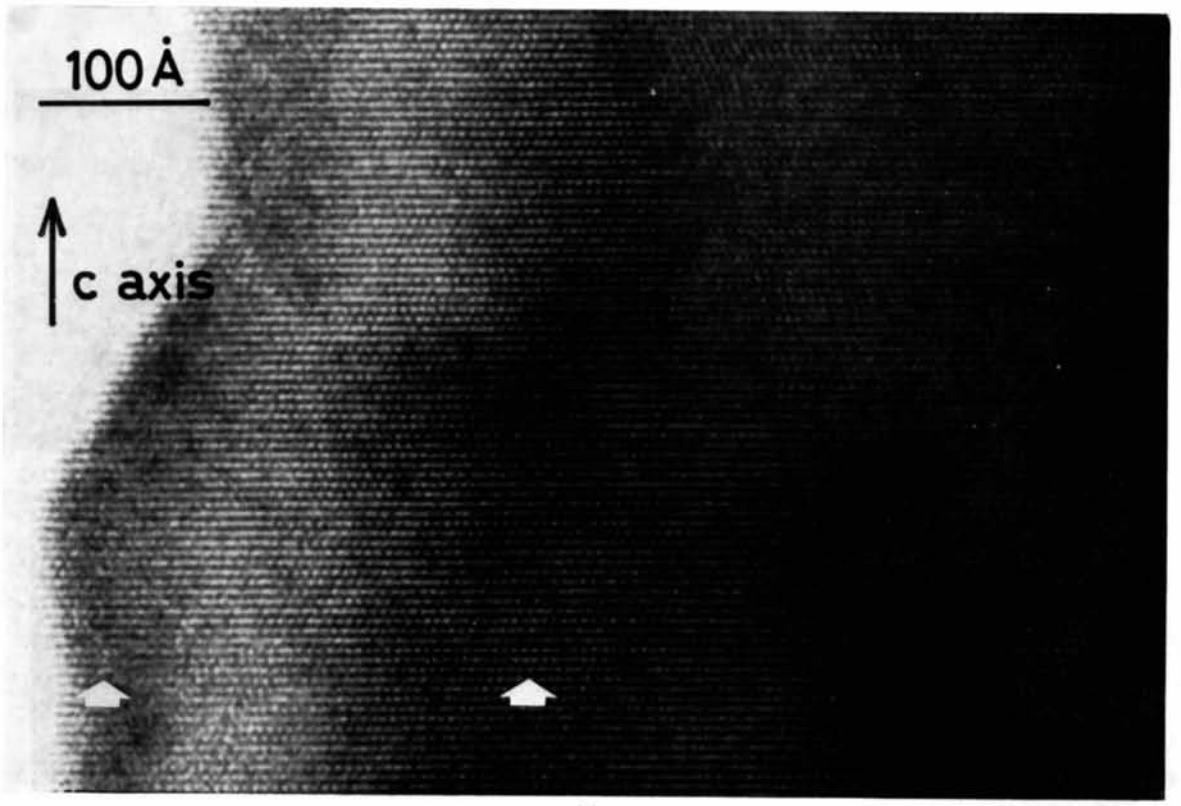

(*a*)

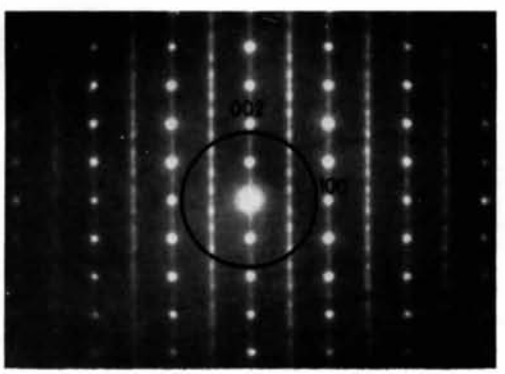

(*b*)

Fig. 5. (*a*) An electron microscope lattice image of a non-stoichiometric vanadium monosulphide, $VS_{1\cdot155}$, with relatively low magnification. Arrows show the first and second equal-thickness contours, whose centres are estimated to be about 60 and 220 Å in thickness, respectively. (*b*) A selected-area diffraction pattern corresponding to (*a*). The circles represent the position and size of the objective aperture used for imaging.

[*To face p.* 560

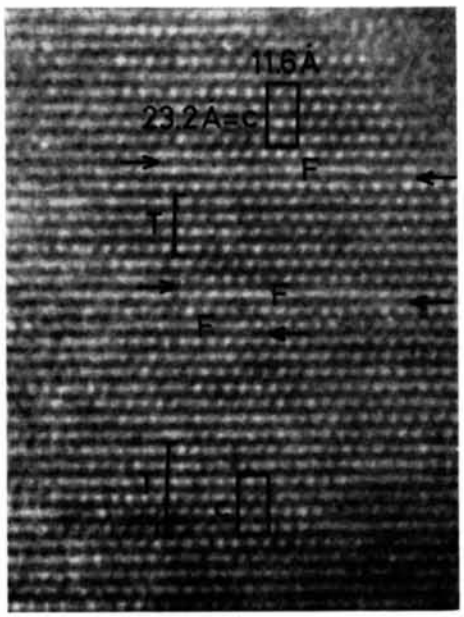

(*a*)

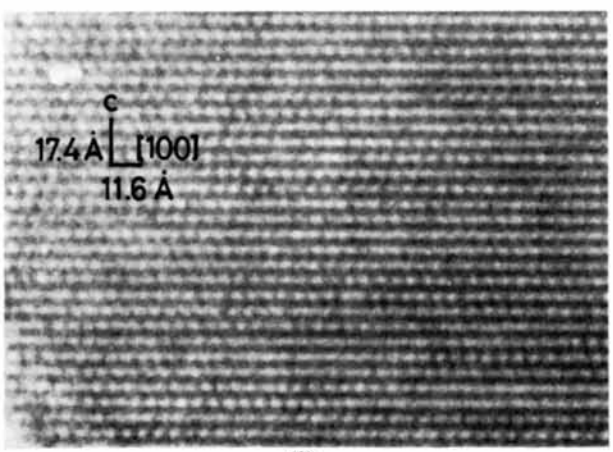

(*b*)

Fig. 6. Lattice images of different parts within a crystal fragment of $VS_{1\cdot155}$. (*a*) shows a 4*C* type superstructure region. (*b*) shows another type of region, where the image is not defined because vacancies have moved in the process of transition from the 3*C* to 4*C* type during cooling of the specimen.

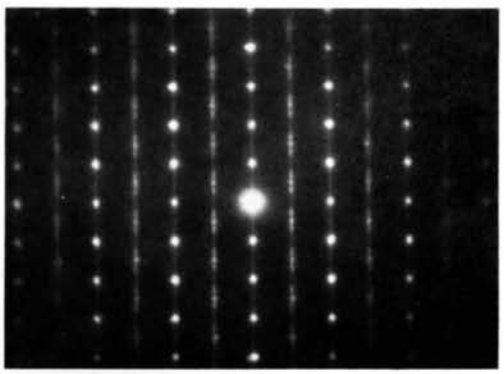

(*a*)

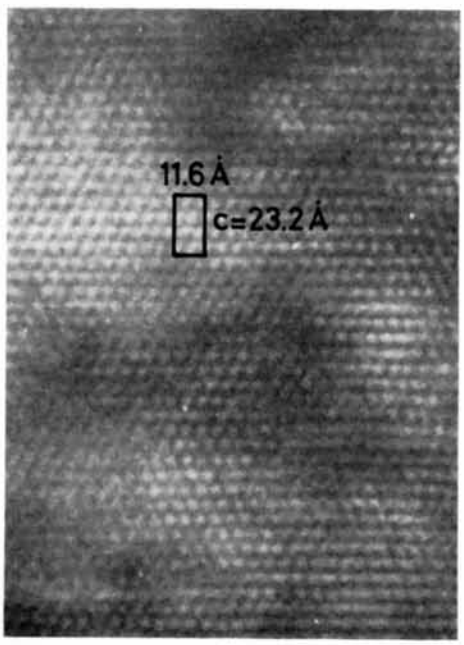

(*b*)

Fig. 7. (*a*) A diffraction pattern and (*b*) an image of the same crystal region as in Fig. 5(*b*) and Fig. 6(*a*), after being heated for a short time by bombardment with an intense electron beam.

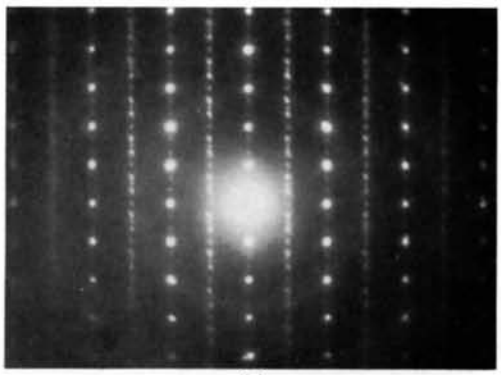

(*a*)

(*b*)

Fig. 8. (*a*) A diffraction pattern and (*b*) an image of the crystal, heated for a long time by bombardment with an intense electron beam.

and aperture size. C_s was taken as 2·0 mm throughout the computation, which seemed reasonable for the present electron microscope equipped with a goniometer stage. Fig. 1(*c*) shows an example of a lattice image computed for the crystal of 120 Å thick. It was obtained at $\Delta f = 900$ Å with the aperture of medium size in Fig. 2, which enabled 11 waves (reflexions *a*, *d*, *e*, *f* and equivalent ones) to contribute to imaging. The magnification is taken as unity. It is evident on comparison with the crystal structure that the rows of vanadium vacancies aligned parallel to the $\mathbf{b}_o$ axis are imaged as white spots, while those of fully occupied vanadiums and of sulphurs are included in the dark matrix without being distinguished from each other. Similar images were obtained for the given limits of thickness and defocus, *e.g.* for a thickness of 80 to 250 Å at an underfocus of 900 to 1200 Å except in the thicker part of the crystal. These limits are represented as the area *G* in Fig. 4 for thickness up to 300 Å. Outside these areas the contrast was modified and no longer corresponded intuitively to the structure model. On large deviation of defocus, *e.g.* at an underfocus of about 300 Å, the image with reversed contrast to Fig. 1(*c*) appeared for a thickness of 100 to 180 Å. The areas of such contrast reversal are also shown by *R* in Fig. 4.

Simulation images were further calculated for two other apertures of different size in Fig. 2. For the smaller aperture images similar to Fig. 1(*c*) were obtained in almost the same extent of defocus and thickness as Fig. 4. On the other hand, for the larger aperture, which enabled the 002 and 100 reflexions of the NiAs subcell to pass, images were severely modified and the areas of *G* and *R* were substantially limited. It can thus be summarized theoretically that vacancy rows are uniquely resolved as white spots when the images are taken with the medium or smaller aperture at an underfocus near 900 Å, not only for the thinnest part of the crystal edge but also to some extent for thicker parts inside the first equal-thickness contour.

Experimental procedure

V_3S_4 block crystals of about 0·5 mm, prepared by means of chemical transport (Saeki & Nakahira, 1974), were reduced by heating at 1217 °C for 4 h under a sulphur partial pressure controlled at 9×10^{-7} torr (Nakano-Onoda & Nakahira, 1976). The crystals were then cooled down in the same atmosphere to room temperature within 1 min. In order to determine the chemical composition some of them were further heated in air at 500 °C and oxidized to V_2O_5. It was calculated to be $VS_{1.155}$ based on weight change on oxidation.

The sulphide crystals gave the fundamental reflexions of NiAs-type with some weak diffuse ones on an X-ray powder diffractometer chart. The lattice parameters of the NiAs subcell were measured to be $A = 3.351$ and $C = 5.814$ Å.

The specimen preparation for lattice image observation and the adjustment of the electron microscope were performed as reported previously (Horiuchi, Saeki, Matsui & Nagata, 1975); the sulphide crystals were crushed in an agate mortar to fragments of about several microns in size. The fragments were set obliquely on a holey carbon supporting film. Observations were made by using a HU 12A-type electron microscope with a goniometer stage operated at the accelerating voltage of 100 kV. The specimens were tilted so that a selected zone axis became parallel to the incident beam. Photographs were usually taken at about 900 Å underfocus. Direct magnification was of about $2{\cdot}5 \times 10^5$ times.

Experimental results and interpretation

Fig. 5(*a*) is an electron microscope image with relatively low magnification, which was taken with the incident beam normal to the (110) plane of the hexagonal supercell. It is characteristic that the first equal-thickness contour appears very near the edge of the crystal fragment. This means that it is not of sharp wedge form. The image outside the contour is neither clear nor regular. Interpretable lattice images appear exclusively in the region inside the first contour.

Fig. 5(*b*) shows a diffraction pattern from the area including that in Fig. 5(*a*). The diffraction spots are indexed based on the NiAs subcell in the figure. In addition to the fundamental reflexions some superstructure spots and streaks parallel to the $\mathbf{c}^*$ axis are found. The $0,0,2n-1$ reflexions must have been excited partly due to the fact that vacancies are confined to every second vanadium layer. The effect of dynamical scattering must be also taken into account (curve *d* in Fig. 3). The intensity maxima in the streaks are located at $(2m-1)/2,0,(2n-1)/4$ and $(2m-1)/2,0,n/3$ and submaxima at $(2m-1)/2,0,(2n-1)/2$, where *m* and *n* are integers. High intensity is continuously distributed between the adjoining maxima to form broad peaks along the c^* axis.

Electron diffraction patterns were also taken with the incident beam normal to the (100) or $(\bar{5}40)$ plane. All of these showed the superstructure reflexions and streaks, which could be explained consistently with Fig. 5(*b*).

X-ray precession photographs of the (*hk*0) reciprocal lattice section were taken from large crystals and they showed the intensity distribution similar to Fig. 5(*b*). This means that the crystal structure was not destroyed through crushing or bombardment by electrons of the minimum intensity necessary for observation.

All the intensity peaks in Fig. 5(*b*) are schematically drawn in Fig. 2; the reflexions at $(2m-1)/2,0,(2n-1)/2$ correspond to the upward triangles in Fig. 2, as mentioned above. Those at $(2m-1)/2,0,(2n-1)/4$ and $(2m-1)/2,0,n/3$ correspond to the downward triangles and open squares, respectively. Detailed accounts for the latter two reflexions are given later.

Fig. 6(*a*) and (*b*) shows two representative lattice images, which were observed in the same crystal fragment as that of Fig. 5, with a large magnification. The objective aperture used in imaging was as indicated in Fig. 5(*b*) and almost the same in size as the medium one in Fig. 2. The arrangement of white spots in Fig. 6(*a*) is similar to that in the simulation image of Fig. 1(*c*). The projection of the unit cell of the 4*C*-type superstructure in the [110] direction can be taken as drawn at the upper part of the figure.

In some regions marked *T*, the arrangement of white spots is different from that mentioned above, *i.e.* two adjacent white spots are often aligned parallel to the *c* axis. It is assumed on the basis of the arrangement of white spots that the stacking sequence of the partially occupied vanadium layers in these regions is changed to $\ldots V_A V_C V_B V_D V_A \ldots$ or $\ldots V_A V_D V_B V_C V_A \ldots$ or equivalent ones. The same assumption was also made by Nakazawa, Morimoto & Watanabe (1975), who tried to interpret the lattice image of Fe_7S_8 intuitively. It is now clear that the assumption is valid for the two reasons: (1) the reflexions expected from the crystal with this orientation are strongly excited in Fig. 5(*b*); they are denoted by downward triangles in Fig. 2. (2) A computer simulation of the lattice image was calculated for this orientation and the result coincided well with the microscope image.

The regions *T* are in a twin relation with the matrix region. The two regions can be crystallographically connected by a mirror relation on a {210} plane or by a 180° rotation about a ⟨210⟩ axis. On twinning, vanadium vacancies have only to change their positions in the intralayers. The twin boundaries are almost parallel to (001) in the present case. The projection of the supercell in the twinned region is also drawn in the figure. Both the matrix or twinned regions extend with band-like form and their thickness is less than 50 Å.

The reflexion intensity from the twinned region is higher than that from the matrix region indicating that the volume of the former is larger than that of the latter in the selected area, from which Fig. 5(*b*) was obtained.

Another type of lattice image, which was not so well defined as above, was found in more than half of the whole crystal observed. In this region white spots were arranged regularly only in quite small areas and often mixed with white lines parallel to $[1\bar{1}0]$. Fig. 6(*b*) represents a typical example, showing that vacancies are confined to every second vanadium layer but considerably disordered in the intralayers. Taking account of the diffraction pattern in Fig. 5(*b*), the crystal in this region must cause the broad peaks between adjoining two maxima (downward triangles and open squares in Fig. 2). The calculation of the structure factors indicates that the reflexions at $(2m-1)/2,0,n/3$ (open squares) are excited from the 3*C*-type superstructure with the stacking sequence of $\ldots V_A V_B V_C V_A \ldots$. The broad peaks are considered to show the presence of some non-integral-type reflexions besides the 4*C* and 3*C* ones. The considerably disordered array of white spots seems to indicate the statistical distribution of vacancies in the intralayers (Koto, 1976) rather than the disordered sequence of antiphase domains (Pierce & Buseck, 1974) in the present non-integral type superstructures. Further discussion on the 3*C*-type structure will be presented later.

Some other crystals, in which the electron beam was incident parallel to the [110] direction, were also examined. Diffraction patterns and lattice images were similar to those in Figs. 5 and 6.

The images were stable as long as the electron beam was kept at the lowest intensity necessary for observation. When the beam intensity was increased by using a larger condenser aperture and by controlling the current of the condenser lens, structural changes occurred in images as well as in diffraction patterns. On irradiation by an intense electron beam the changes proceeded abruptly and the image became indistinct. This is considered to be firstly due to the fact that the temperature gradient is very steep in the small area under observation and yields complex thermal strain and secondly due to all the possible effects of electron bombardment (Heidenreich, 1964) including specimen contamination. In order to overcome this difficulty the electron beam was condensed to a portion which is a few microns away from the region under examination. The selected region was thus heated not by direct electron bombardment but by heat conduction. This method allowed an almost uniform temperature rise at the region without radiation damage to the crystal. The structural changes could then be controlled. When the condenser aperture was reset to the initial small size, the changes immediately stopped. This means that the specimen cooled very rapidly. Images were taken after recorrecting the focus and astigmatism.

The diffraction pattern had changed in two stages. Fig. 7(*a*) and Fig. 8(*a*) show typical diffraction patterns at an intermediate and at an advanced stage of heating, taken from the same portion of the crystal as that used for Fig. 5(*b*). Fig. 7(*a*) was attained after heating for 10 s by an intense electron beam. Intensity peaks at $(2m-1)/2,0,(2n-1)/2$ became stronger, while the streaks parallel to the c^* axis were still retained with sufficient intensity. This means that the 4*C*-type superstructure with the matrix orientation became predominant in volume in the portion observed.

Fig. 7(*b*) is an image corresponding to Fig. 7(*a*). The image was taken from exactly the same area as that of Fig. 6(*a*). The arrangement of white spots indicates the presence of the 4*C*-type superstructure with the matrix orientation in almost the whole area of the photograph.

Fig. 8(*a*) shows a diffraction pattern at the advanced stage of heating with the most intense electron beam for 2 min without a condenser aperture. It is noted that superstructure reflexions became discrete, *i.e.* streaks

became weaker. The diffraction spots at $(2m-1)/2,0,n/3$ are strong, while those at $(2m-1)/2,0,(2n-1)/2$ are weaker. Those at $(2m-1)/2,0,(2n-1)/4$ are weak and split in the $[1\bar{1}0]$ direction. It is moreover noted that new extra spots appear at $m,0,n/3$; these are shown by filled squares in Fig. 2.

Fig. 8(*b*) represents an image corresponding to Fig. 8(*a*). Every third white line shows brighter contrast. The periodicity is consistent with that observed in the diffraction pattern above. The contrast anomaly is considered to suggest that the vacancy concentrations are different in each partially occupied vanadium layer. The rearrangement of vacancies in the intralayers and the strain field induced must be responsible for the observation that sharp white spots are regularly arrayed only partly in some layers. The arrangement of white spots at the parts underlined is similar to that of the stacking faults discussed later concerning Figs. 6 and 10. No information corresponding to the split reflexions at $(2m-1)/2,0,(2n-1)/4$ was obtained in the images.

Discussion

No crystal fragment whose orientation was suitable for observation by the lattice image technique was of sharp wedge form, *i.e.* the equal-thickness contour was found very near the edge of the fragment. This may be correlated to the indication that the cleavage during crushing occurs parallel to the (001) plane, as expected based on the crystal structure. The situation is different from that for some oxides like Nb_2O_{5-x} (Iijima, 1973; Horiuchi & Matsui, 1974), in which the fragment had sometimes a large, thin area at the edge. For sulphides as in the present case as well as Fe_7S_8 (Nakazawa, Morimoto & Watanabe, 1975), in which interpretable lattice images also appeared only at the thicker part of the crystal, the intuitive interpretation of the image is thus no longer applicable. The dynamical treatment of scattering is necessary for correct evaluation of the image contrast.

It was shown by the dynamical calculation that the rows of vacancies were imaged as white spots even at the thicker part of crystal when the conditions of defocus and aperture size were fulfilled. The contrast was observed to reverse when the defocus was changed to about 300 Å underfocus in accordance with the results of the computer simulation.

The kinematical calculation was performed prior to the dynamical one so far described. The simulation images obtained from the former were qualitatively in accordance with those from the latter for a thickness of less than 30 Å, provided the same defocus and aperture size were taken into account.

The effect of absorption in the crystal was so far neglected. It can be taken into account by introducing the imaginary part into the crystal potential (Goodman & Lehmpfuhl, 1967). The transmission function was here approximated by $\exp[i\sigma(1+i\alpha)\varphi(x,z)]$, where α is a constant value. The amplitudes were dynamically calculated with this function for some values of α up to 0·2. The intensity and phase obtained is represented in Fig. 9 for $\alpha=0{\cdot}1$, for which the intensity profile in the image in Fig. 5(*a*) can be fitted fairly well. The sums of the intensities of all the transmitted and diffracted waves at the thickness of 500 Å was 0·91, 0·30, 0·18 and 0·065 for $\alpha=0{\cdot}0$, 0·05, 0·1 and 0·2, respectively.

The lattice images were calculated for the case of $\alpha=0{\cdot}1$. It was shown that the effects of thickness (< 300 Å), defocus and aperture size were very similar to those mentioned for $\alpha=0{\cdot}0$.

In the matrix of the 4*C*-type superstructure white spots sometimes link together in the $[1\bar{1}0]$ direction to appear as white lines marked *F* in Fig. 6(*a*). Some stacking faults are found at the position arrowed near the lines; the rows of vacancies around a white line are considered to be arranged as schematically shown in Fig. 10(*a*); the stacking sequence is assumed to be $\ldots V_A V_B V_C V_A \ldots$ in the left region and $\ldots V_A V_B V_D V_A \ldots$ in the right one. The boundary between the two regions lies obliquely to the [110] direction. In the third layer the arrangement of vacancy rows is not coherently connected at the boundary. For the supercell outlined in the figure the image contrast was calculated with a total thickness of 120 Å; the incident

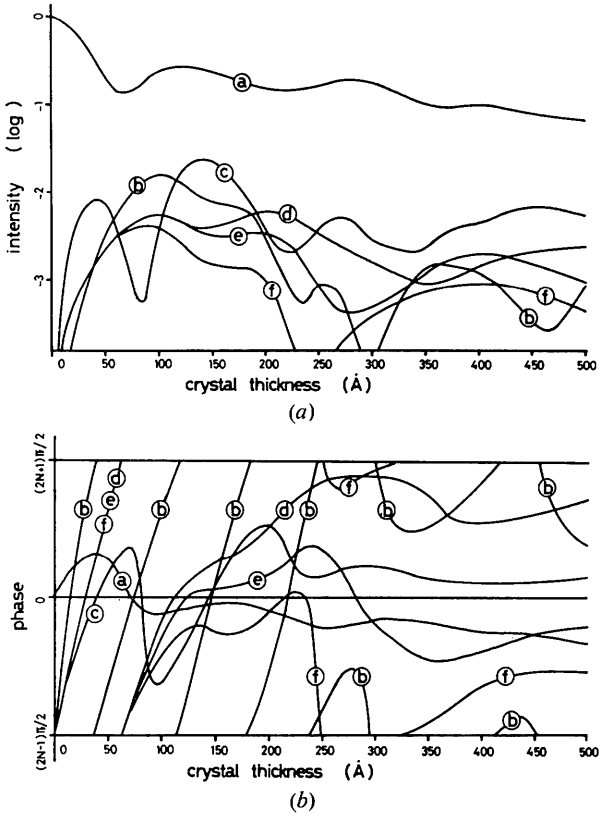

Fig. 9. (*a*) intensity and (*b*) phase, calculated taking into consideration absorption. The projected potential of a slice is assumed as $(1+0{\cdot}1i)\varphi(x,z)$. Compare with Fig. 3, where no absorption has been taken into account.

beam parallel to the [110] direction is scattered first by the crystal with a stacking sequence of $\ldots V_A V_B V_C V_A \ldots$ for the thickness of 60 Å and then, after passing across the boundary, by that of $\ldots V_A V_B V_D V_A \ldots$ for the subsequent 60 Å. The result obtained is shown in Fig. 10(*b*). It is clear that the third layer is imaged as a white line with less bright contrast.

DeVries (1972) has reported the 4*C*-type superstructure for $VS_{1.12}$, prepared at 800°C and cooled slowly. On the other hand, Grønvold *et al.* (1969) have found extra X-ray reflexions at the position of $l=\frac{1}{2}$ for $VS_{1.150}$, prepared and quenched at 800°C, and suggested the presence of a 2*C*-type superstructure. Although they have not proposed any structure for the 2*C* type, it may be assumed to be $\ldots V_A V_B V_A \ldots$ or $\ldots V_C V_D V_C \ldots$ or *etc.* This type of structure would explain not only the extra reflexions at $l=\frac{1}{2}$ but also the lattice images, observed at the first stage of heating [Fig. 7(*a*) and (*b*)]. The presence of such a superstructure is however denied for the following reasons; (1) the structures such as $\ldots V_A V_C V_A \ldots$ or $\ldots V_B V_D V_B \ldots$ or *etc.*, which are crystallographically equivalent to $\ldots V_A V_B V_A \ldots$ or $\ldots V_C V_D V_C \ldots$ or *etc.* and therefore must be formed with equal probability, could give no reflexions at $l=\frac{1}{2}$ in the (110) reciprocal lattice section. (2) No images, which correspond to the structure such as $\ldots V_A V_C V_A \ldots$ or $\ldots V_B V_D V_B \ldots$ or *etc.*, were observed clearly throughout the heating process. (3) Any type either of $\ldots V_A V_B V_A \ldots$ or $\ldots V_A V_C V_A \ldots$ requires a closer proximity of vacancies and would seem to be unstable with respect to the 4*C* type. It is therefore concluded that the 2*C* type was not formed and the 4*C* type has changed directly to the 3*C* type with the increase of temperature.

The fact that the 3*C* type is more stable at high temperature than the 4*C* type has also been reported for Fe_7S_8 (Fleet, 1971) and Fe_7Se_8 (Okazaki, 1961). In the latter case the 3*C* type was proposed to have the structure with stacking sequence type $\ldots V_A V_B V_C V_A \ldots$. In Fig. 8(*b*) stacking faults seemed to be formed at the plane marked by lines and the structure of the limited region including the lines must be of the 3*C* type. As mentioned above, however, this type gives the reflexions only at $(2m-1)/2,0,n/3$ (open squares in Fig. 2). The calculation of the structure factors on the following model provides a useful suggestion; if a small fraction of vacancies move from a partially occupied vanadium layer to another and the vacancy concentration is no longer constant among the layers, the additional reflexions at $m,0,n/3$ (filled squares in Fig. 2) are excited, as detected in Fig. 8(*a*). It may be reasonable to consider that this fluctuation in the vacancy concentration was observed as the contrast anomaly in Fig. 8(*b*).

The phase relation is summarized as follows; at high temperature, probably higher than 800°C, the 3*C*-type superstructure is stable. As the specimen is cooled vacancies move in the inter- as well as intralayers. The rate of vacancy movement differs from region to region. In the region cooled relatively slowly the 4*C*-type superstructure, which is stable at lower temperature, is produced. Other regions are occupied by the complex structures, which occur during the transition from the 3*C* to 4*C* type [Fig. 6(*b*)].

Desulphurization was not remarkable during observation. This may be because a carbon contamination layer covered the crystal surface. Moreover, no reaction of the crystal with the carbon was detected, *i.e.* no carbides were identified on the diffraction pattern. When the observation was prolonged, the image became indistinct and the diffraction pattern occasionally included only $m,0,2n-1$ spots without any streaks or any other superstructure reflexions. This is interpreted as showing that the interlayer ordering was still retained although no intralayer ordering was any longer maintained. It has been shown for a higher vanadium sulphide, V_5S_8, that vacancies were still partially ordered in the interlayers even at high temperatures, at which they were completely disordered in the intralayers (Nakazawa, Saeki & Nakahira, 1975).

The authors wish to express their deep gratitude to Mr M. Saeki for providing the starting block crystals of V_3S_4. Their thanks are also due to the referee for his constructive criticism.

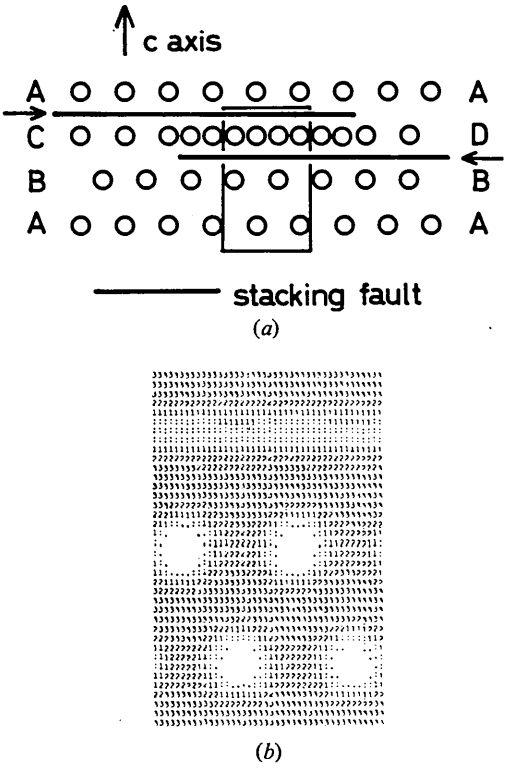

Fig. 10. (*a*) Schematic representation of the contrast at a position *F* in Fig. 6(*a*) by white spots. (*b*) Computer simulation image of the crystal region outlined in (*a*). The thickness is taken as 120 Å.

References

ALLPRESS, J. G. & SANDERS, J. V. (1973). *J. Appl. Cryst.* **6**, 165–190.

ALLPRESS, J. G., SANDERS, J. V. & WADSLEY, A. D. (1969). *Acta Cryst.* B**25**, 1156–1164.

BERTAUT, E. F. (1953). *Acta Cryst.* **6**, 557–561.

BUSECK, P. R. & IIJIMA, S. (1974). *Amer. Min.* **59**, 1–21.

COWLEY, J. M. & IIJIMA, S. (1972). *Z. Naturforsch.* **27**a, 445–451.

COWLEY, J. M. & MOODIE, A. F. (1957). *Acta Cryst.* **10**, 609–619.

DEVRIES, A. B. (1972). Dissertation, Univ. Groningen, Netherlands.

EISENHANDLER, C. B. & SIEGEL, B. M. (1966). *J. Appl. Phys.* **37**, 1613–1620.

FLEET, M. E. (1971). *Acta Cryst.* B**27**, 1864–1867.

GOODMAN, P. & LEHMPFUHL, G. (1967). *Acta Cryst.* **22**, 14–24.

GOODMAN, P. & MOODIE, A. F. (1974). *Acta Cryst.* A**30**, 280–290.

GRØNVOLD, F., HARALDSEN, H., PEDERSEN, B. & TUFTE, T. (1969). *Rev. Chim. Min.*, **6**, 215–240.

HEIDENREICH, R. D. (1964). In *Fundamentals of Transmission Electron Microscopy*, p. 165. New York: Interscience.

HORIUCHI, S. & MATSUI, Y. (1974). *Phil. Mag.* **30**, 777–787.

HORIUCHI, S., MATSUI, Y., KATO, K. & NAGATA, F. (1975). *Jap. J. Appl. Phys.* **14**, 1837–1838.

HORIUCHI, S., SAEKI, M., MATSUI, Y. & NAGATA, F. (1975). *Acta Cryst.* A**31**, 660–664.

IIJIMA, S. (1971). *J. Appl. Phys.* **49**, 5891–5893.

IIJIMA, S. (1973). *Acta Cryst.* A**29**, 18–24.

IIJIMA, S., KIMURA, S. & GOTO, M. (1973). *Acta Cryst.* A**29**, 632–636.

KAWADA, I., NAKANO-ONODA, M., ISHII, M., SAEKI, M., & NAKAHIRA, M. (1975). *J. Solid State Chem.* **15**, 246–252.

KOTO, K. (1976). To be published.

LYNCH, D. F., MOODIE, A. F. & O'KEEFE, M. A. (1975). *Acta Cryst.* A**31**, 300–307.

NAKANO-ONODA, M. & NAKAHIRA, M. (1976). To be published.

NAKAZAWA, H., MORIMOTO, N. & WATANABE, E. (1975). *Amer. Min.* **60**, 359–366.

NAKAZAWA, H., SAEKI, M. & NAKAHIRA, M. (1975). *J. Less-Common Met.* **40**, 57–63.

OKAZAKI, A. (1961). *J. Phys. Soc. Japan*, **16**, 1162–1170.

O'KEEFE, M. A. (1973). *Acta Cryst.* A**29**, 389–401.

PIERCE, L. & BUSECK, P. R. (1974). *Science*, **186**, 1209.

SAEKI, M. & NAKAHIRA, M. (1974). *J. Cryst. Growth*, **24/25**, 154–157.

SCHERZER, O. (1949). *J. Appl. Phys.* **20**, 20–29.

UYEDA, N., KOBAYASHI, T., SUITO, E., HARADA, Y. & WATANABE, M. (1972). *J. Appl. Phys.* **43**, 5181–5189.

Acta Cryst. (1976). A**32**, 565

Electron Population Analysis with Rigid Pseudoatoms

BY ROBERT F. STEWART*

Department of Chemistry, Carnegie-Mellon University, 4400 *Fifth Avenue, Pittsburgh, Pennsylvania*, 15213, *U.S.A.*

(*Received* 21 *July* 1975; *accepted* 30 *January* 1976)

The one-electron density function for a group of atoms within the asymmetric region of a unit cell is represented by a finite multipole expansion of the charge density about each atomic center. Each atomic expansion is called a pseudoatom. If the pseudoatom charge density is effectively rigid with nuclear motion, then the model may be used for a static charge density analysis of X-ray diffraction data. A valence density multipole model for pseudoatoms is restricted to single exponential radial functions. The representation is rotationally invariant. The model may be used for determination of static charge physical properties as well as aspects of chemical bonding. These results can be a critical test of the X-ray diffraction experiment for the determination of electron density distributions. The pseudoatoms discussed are primarily intended for crystals comprised of first and second-row atoms. The valence scattering model demands extensive data sets (probably at low temperatures) or an independent determination of atomic positions and mean square amplitudes of vibration.

Introduction

Over the last few years several models for a quantitative determination of electron density distributions from X-ray diffraction data have been proposed. Dawson (1967) proposed an atom deformation model which was extended by Kurki-Suonio (1968). Hirshfeld (1971) and Harel & Hirshfeld (1975) have applied the model to electron density analysis of organic molecular crystals. The model is a representation of the one-electron density function in the asymmetric part of the unit cell with a finite multipole expansion about the several atomic centers.

In the present paper several facets of the multipole model are reviewed within the framework of the fundamental theory for coherent X-ray scattering intensities. Several features of the model have been published in fragmentary reports by the author and by other workers. The effort here is an attempt to present the concept of pseudoatoms (or generalized X-ray

* Alfred P. Sloan Fellow.